Rapid Communications

Emergent excitability in populations of nonexcitable units

Marzena Ciszak,[1] Francesco Marino,[1,2] Alessandro Torcini,[3,4] and Simona Olmi[5,4,2,*]

[1]*CNR - Consiglio Nazionale delle Ricerche - Istituto Nazionale di Ottica, Via Sansone 1, I-50019 Sesto Fiorentino (FI), Italy*

[2]*INFN, Sezione di Firenze, Via Sansone 1, I-50019 Sesto Fiorentino (FI), Italy*

[3]*Laboratoire de Physique Théorique et Modélisation, Université de Cergy-Pontoise, CNRS, UMR 8089, F-95302 Cergy-Pontoise Cedex, France*

[4]*CNR - Consiglio Nazionale delle Ricerche - Istituto dei Sistemi Complessi, via Madonna del Piano 10, I-50019 Sesto Fiorentino, Italy*

[5]*Inria Sophia Antipolis Méditerranée Research Centre, 2004 Route des Lucioles, F-06902 Valbonne, France*

(Received 17 July 2020; accepted 10 November 2020; published 20 November 2020)

Population bursts in a large ensemble of coupled elements result from the interplay between the local excitable properties of the nodes and the global network topology. Here, collective excitability and self-sustained bursting oscillations are shown to spontaneously emerge in globally coupled populations of nonexcitable units subject to adaptive coupling. The ingredients to observe collective excitability are the coexistence of states with different degrees of synchronization joined to a global feedback acting, on a slow timescale, against the synchronization (desynchronization) of the oscillators. These regimes are illustrated for two paradigmatic classes of coupled rotators, namely, the Kuramoto model with and without inertia. For the bimodal Kuramoto model we analytically show that the macroscopic evolution originates from the existence of a critical manifold organizing the fast collective dynamics on a slow timescale. Our results provide evidence that adaptation can induce excitability by maintaining a network permanently out of equilibrium.

DOI: 10.1103/PhysRevE.102.050201

Introduction. Complex networks composed of simple elements, usually rotators, have been widely analyzed in the last decades in order to identify the emergence of nontrivial macroscopic phenomena, ranging from synchronization to collective oscillations, quasiperiodicity, and chaos [1–6]. The field has particularly flourished in the last years owing to the development of analytic techniques to obtain exact low-dimensional mean-field descriptions for phase oscillator networks [7].

Despite this intense activity only a few analyses have reported signatures of collective excitable features in such networks [8,9]. Excitable systems appear in many fields of science and are particularly studied in the context of mathematical neuroscience as simplified descriptions of neural systems [10,11]. They are characterized by a (quiescent) state that is linearly stable, but susceptible to finite-amplitude perturbations. The return to equilibrium entails a large excursion in the phase space corresponding to the emission of a pulse of well-defined amplitude and duration. The reinjection mechanism to the excitable quiescent state is often related to the competition of multiple timescales [12]. The dynamical scenario emerging in these low-dimensional slow-fast systems can be extremely rich, displaying regular as well as chaotic spiking and bursting behaviors joined to complex bifurcation structures [13–18].

Collective excitable responses and bursting activities have been previously reported [19], e.g., in diffusively coupled, spatially extended systems where they appear in the form of excitable waves [20], as transient synchronization states in arrays of coupled units [21,22]. In all these cases, however, the dynamics fully relies on excitable features of the nodes.

In this Rapid Communication we show that a self-sustained adaptation mechanism can give rise to an out-of-equilibrium scenario, where a population of nonexcitable nodes, permanently driven across a hysteretic phase transition, can become collectively excitable. In particular, we investigate the effects of a global linear feedback on the dynamics of the Kuramoto model (KM) with and without inertia. In the absence of adaptation, the considered networks display hysteretic first-order transitions involving asynchronous (AS) and partially synchronized (PS) states, as well as standing waves [23–26]. In the presence of the feedback, these systems reveal collective dynamical features typical of excitable models, despite a nonexcitable single-node dynamics. The origin of these behaviors is related to the competition of the fast synchronization/desynchronization phenomena triggered by the slow adaptation. For the bimodal KM, we derive an exact three-dimensional slow-fast mean-field formulation, which allows us to interpret all the observed collective regimes in terms of an attractive invariant manifold, on which the (slow) mean-field dynamics takes place. Finally, these phenomena are shown to emerge also in the Kuramoto model with inertia (KMI), confirming the generality of our results.

The model. We consider a globally coupled population of N rotators with adaptive coupling strength $S(t)$, which reads as

$$m\ddot{\theta}_l + \dot{\theta}_l(t) = \omega_l + \frac{S(t)}{N}\sum_{j=1}^{N}\sin[\theta_j(t) - \theta_l(t)], \quad (1a)$$

$$\dot{S}(t) = \varepsilon[-S(t) + K - \alpha R(t)], \quad (1b)$$

*Corresponding author: simona.olmi@fi.isc.cnr.it

 ©2020 American Physical Society

where θ_l (ω_l) are the phases (natural frequencies) of each rotator and m their mass. As stated in Eq. (1b), the evolution of $S(t)$ is controlled, via a linear feedback [9], by $R(t)$, which is the modulus of the complex Kuramoto order parameter $Z(t) = \frac{1}{N}\sum_{j=1}^{N} e^{i\theta_j(t)} = R(t)e^{i\Phi(t)}$ [27]. The macroscopic variable R measures the level of synchronization among the rotators: AS (PS) dynamics will correspond to $R = 0$ ($0 < R \leqslant 1$). The gain of the feedback loop is controlled by α and its bandwidth by ε, therefore, depending on the value of $R(t)$, the coupling $S(t)$ can range between $K - \alpha$ ($R = 1$) and K ($R = 0$). We assume $0 < \varepsilon \ll 1$, i.e., the modulation of the coupling is slow with respect to the switching times between incoherent and coherent states.

In the absence of feedback ($\alpha = 0$), Eq. (1a) reduces to the KMI with coupling constant $S(t) \equiv K$ [25] and for $m = 0$ to the standard KM [27]. For both these models, at sufficiently low (large) coupling, one has a desynchronized (partially synchronized) regime. If the transition from AS to PS dynamics is continuous, as for the KM with unimodal frequency distribution, the feedback (1b) has only the effect to rescale the coupling strength, but the collective dynamics will always converge to a stable fixed point for all the parameter values. This is no longer the case if the uncontrolled system displays a first-order hysteretic transition from incoherence to coherence, as it occurs for the KMI [25,26,28] and for the KM with a bimodal frequency distribution [24]. In this case, the linear feedback introduced above can give rise to a wealth of macroscopic behaviours over multiple timescales, including excitability and periodic/chaotic spiking and bursting oscillations.

KM with bimodal frequency distribution. As our first paradigmatic example of networks displaying hysteretic phase transitions, we consider the KM with a bimodal distribution of natural frequencies [24]. In particular, in order to be able to derive an exact mean-field description of the model we consider a bimodal distribution given by the sum of two Lorentzians centered at $\pm\omega_0$ and with half width at half maximum Δ [29]. For the chosen parameters ($\omega_0 = 1.8$ and $\Delta = 1.4$), in the absence of feedback, we observe a coexistence regime between traveling waves and PS states [30]. By fixing a finite feedback gain α and the frequency cutoff ε and increasing the control parameter K, we observe the sequence of macroscopic regimes displayed in Fig. 1 in terms of the synchronization parameter $R(t)$.

At small K values the population is essentially desynchronized, apart finite-size fluctuations associated with $R \simeq O(1/\sqrt{N})$. For K larger than a critical value, one observes the emergence of periodic collective oscillations, alternating PS phases with abrupt desynchronization events (*spikes*), as shown in Fig. 1(a). Further increasing K leads first to an increase of the interspike period and then to a chaotic phase [see Fig. 1(b)]. In the chaotic and periodic spiking regimes the system is excitable: Small perturbations of the collective variable $S(t)$ elicit rapidly decaying responses in $R(t)$ (blue traces), while sufficiently strong stimuli induce a large degree of synchronization, corresponding to a *burst* with a well-defined shape, amplitude, and duration [red traces in Figs. 1(a) and 1(b)]. In Fig. 1(b) we also show that, except for the initial rise time, the burst orbit is barely affected by higher-amplitude perturbations (green trace), thus confirming an important feature of excitable systems. The chaotic nature of the spiking dynamics can be appreciated in Fig. 1(b), where in response to perturbations of different amplitudes, the system relaxes to different final trajectories, in contrast to what is shown in Fig. 1(a) for a periodic spiking regime. By further increasing the parameter K one observes the emergence of a regime characterized by the presence of bursts separated by many spikes, whose number appears to be irregular [Fig. 1(c)]. This bursting phase is chaotic, as we will verify in the following. As shown in Fig. 1(d), a further increase of K leads to a periodic bursting state, where the bursts are separated by a fixed number of spikes. The number of spikes decreases for growing K and finally we observe a stationary regime characterized by a finite value of R for sufficiently large K. Similar spiking and bursting regimes, as well as period adding sequences, are typical for low-dimensional slow-fast systems possessing some attractive manifolds on which the dynamics evolves slowly. In this context, a paradigmatic example is represented by the Hindmarsh-Rose neuronal model [13,18]. Similarly, in our network, collective excitability and bursting phenomena originate from the existence of a critical manifold which organizes the mean-field dynamics on the slow timescale, as we will show below.

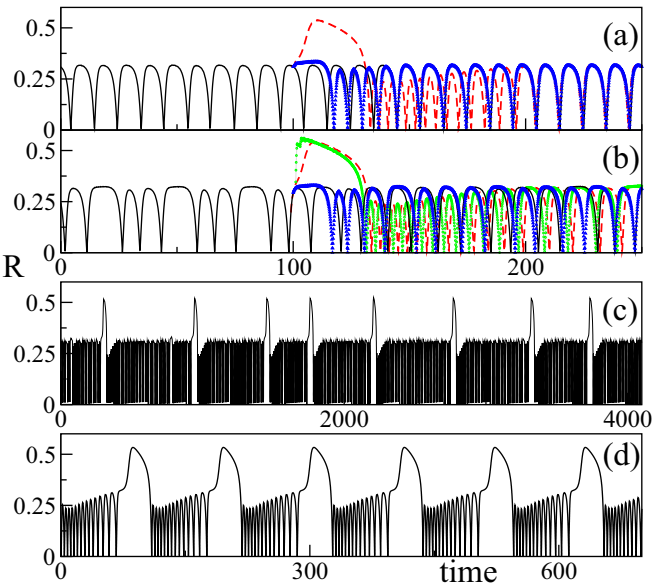

FIG. 1. Synchronization parameter R vs time for the bimodal Kuramoto network for different dynamical regimes: (a) periodic spiking ($K = 7$); (b) chaotic spiking ($K = 7.403$); (c) chaotic bursting ($K = 7.405$); (d) periodic bursting ($K = 7.41$). (a) and (b) display also the system response to perturbations of different amplitudes A of the collective variable $S(t)$: subthreshold responses for $A = 0.102\,55$ (blue triangle-shaped traces); excitable responses for $A = 0.15$ (dashed red traces) and $A = 0.1575$ (dotted green trace). Other parameters: $\varepsilon = 0.01$, $\Delta = 1.4$, $\omega_0 = 1.8$, $\alpha = 5$, and network size $N = 500\,000$.

Exact mean-field analysis. To better understand the observed phenomenology we derive an exact mean-field dynamics for the network (1a), by extending the macroscopic formulation derived in Refs. [8,30] for the bimodal KM, based on the Ott-Antonsen ansatz [7] (for details, see the Supplemental Material [31]). In particular, by following Ref. [30],

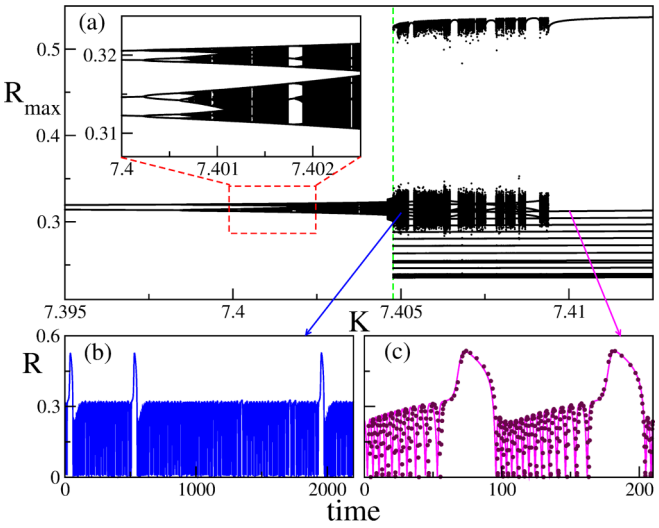

FIG. 2. (a) Bifurcation diagram of the mean-field model (1a). The maxima of R are displayed as a function of the parameter K. Time traces of R for the mean-field model are shown in (b) for the chaotic bursting regime ($K = 7.405$) and in (c) for the periodic bursting phase ($K = 7.41$). Symbols in (c) are the R values estimated by the direct simulation of the network (1a) of size $N = 500\,000$. The (green) dashed vertical line in (a) refers to K_c. Other parameters: $\varepsilon = 0.01$, $\omega_0 = 1.8$, $\Delta = 1.4$, $\alpha = 5$.

one can rewrite the complex order parameter Z in terms of two subpopulation order parameters $z_k = \rho_k e^{i\phi_k}$ $(k = 1, 2)$, each relative to a Lorentzian distribution, as $Z = \frac{1}{2}(z_1 + z_2)$. Moreover, by assuming $\rho_1 \approx \rho_2 = \rho$, one arrives at the following equations ruling the macroscopic evolution of the network,

$$\dot{\rho} = -\Delta\rho + \frac{S}{4}\rho(1-\rho^2)[1+\cos(\phi)], \tag{2a}$$

$$\dot{\phi} = 2\omega_0 - \frac{S}{2}(1+\rho^2)\sin(\phi), \tag{2b}$$

$$\dot{S} = -\varepsilon\left[S - K + \alpha\rho\sqrt{\frac{1+\cos(\phi)}{2}}\right], \tag{2c}$$

where $\phi = \phi_2 - \phi_1$ and the global feedback equation (2c) directly follows from (1b) by noticing that $R \equiv \rho\sqrt{[1+\cos(\phi)]/2}$.

The dynamics of the mean-field model (1a) is attracted towards a stable fixed point corresponding to an AS regime ($R = 0$) for $K < K_H = 4\Delta$, while at K_H a supercritical Hopf bifurcation takes place giving rise to a stable limit cycle (periodic spiking). As shown in Fig. 2(a), the Hopf bifurcation is followed by a period doubling cascade leading to a chaotic spiking regime for $K > 7.401$. Both the regular and chaotic spiking oscillators display excitable features analogous to the collective ones displayed in Figs. 1(a) and 1(b) for the corresponding network. At $K_c \simeq 7.404\,77$, we observe an abrupt increase of the size of the attractor for R, that corresponds to the appearance of chaotic bursts. This transition resembles a crisis that destabilizes the chaotic attractor associated with the spiking phase, leading to the emergence of a new chaotic attractor characterized by bursting dynamics, as shown in Fig. 2(b). Similar transitions have been reported for single excitable systems in Refs. [15,17]. Moreover, we have measured the maximal Lyapunov exponent λ_m [32] for the mean-field model (1a) and observed that this is positive for $K \in [7.401, 7.408]$, a region containing the transition point K_c (see Fig. S2 in the Supplemental Material [31]). This demonstrates that we can have collective chaos [5,6,33,34] also for a single Kuramoto population with a self-generated collective adaptation and not only in the presence of an external periodic forcing [8] or for multiple coupled populations [35]. Furthermore, λ_m shows a pronounced peak in correspondence to $K \simeq K_c$, similarly to what was reported in Ref. [18] for the single Hindmarsh-Rose model. For $K > 7.408$ we observe periodic bursting attractors, as the one reported in Fig. 2(c) for the mean-field model. In Fig. 2(c) are also reported the data obtained from the network, for the macroscopic indicator R: The excellent agreement confirms the validity of the mean-field reduction. For larger K we observe a decrease in the number of spikes separating two successive periodic bursts up to $K = 8.158\,43$ when the system returns to a stable fixed point with $R > 0$ via a subcritical Hopf bifurcation.

Geometric singular perturbation analysis of the mean-field model. Since $\varepsilon \ll 1$, the adaptive variable S evolves at a much slower rate than ϕ and ρ. Hence the dynamics of Eqs. (1a) splits into periods of fast and slow motion that can be analyzed separately [36]. On the fast timescale t, the evolution is described by the mean-field equations (2a) and (2b) (fast subsystem) with S acting as a slowly varying adiabatic parameter. The equilibria of this dynamical subsystem lie on the one-dimensional manifold $\Sigma = \Sigma_0 \cup \Sigma_\rho$, where Σ_0 is given by the set of incoherent steady-state solutions $\Sigma_0 = \{\rho_s = 0, \sin(\phi_s) = 4\omega_0/S, S\}$, and $\Sigma_\rho = \{\rho_s, \phi_s, S\}$ is defined by the equations $S(1+\rho_s^2)\sin(\phi_s) = 4\omega_0$ and

$$S = \frac{2\omega_0^2}{\Delta}\frac{1-\rho_s^2}{(1+\rho_s^2)^2} + \frac{2\Delta}{1-\rho_s^2} \equiv \mathcal{F}(\rho_s). \tag{3}$$

On the slow timescale $\tau = \varepsilon t$, the motion is governed by the feedback equation Eq. (2c) with the algebraic constraint $(\dot{\rho}, \dot{\phi}) = (0, 0)$. The fixed points of the fast subsystem thus define the critical manifold on which the slow dynamics take place. Since the trajectories of Eqs. (2a) and (2c) will be attracted by the stable parts of Σ, while they will be repelled by the unstable ones [37], the stability properties of the critical manifold determine the dynamics. Linearizing the fast subsystem on Σ_ρ, we find that it consists of a branch of stable equilibria Σ_S (solid line in Fig. 3) and an unstable one Σ_R (dashed line) coalescing in a saddle-node bifurcation at the fold point F.

For $\omega_0 > \Delta$, the equilibria along Σ_0 (i.e., for $S > 4\omega_0$) are always unstable. At lower values of S, the fast subsystem (2a) and (2b) displays a supercritical Hopf bifurcation at $S_H = K_H$, leading to the emergence of a stable limit cycle with $\rho > 0$.

The critical manifold is thus composed by an attracting part Σ_S and two repelling parts Σ_R and Σ_0. Moreover, for some values of the slow variable, the above stationary states coexist with a multiplicity of stable limit cycles emanating from the Hopf bifurcation at K_H. On this basis, we can explain the appearance of bursting in our system. In Fig. 3(a) we plot the projection of the critical manifold on the (ρ, S) plane together

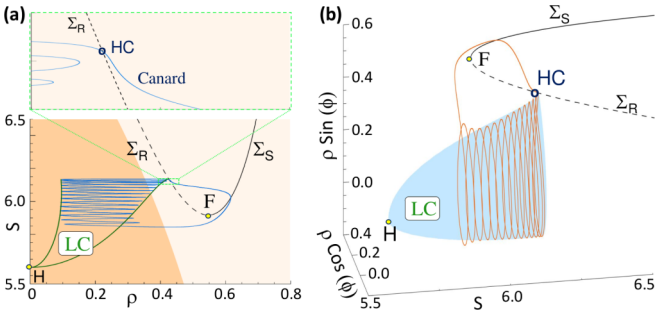

FIG. 3. Critical manifold of the mean-field equations (2a) and (2c) together with a bursting solution (blue solid line). (a) Projection on the (ρ, S) plane: Solid and dashed black lines indicate the attracting (Σ_S) and repelling (Σ_R) manifolds, separated by the fold point F. In the orange-shaded area, $\dot{S} > 0$. The green curves denote the extrema of the limit cycle (LC) emerging from the Hopf bifurcation H. Inset: Enlarged view of the transition region from the spiking regime towards Σ_S occurring via a saddle homoclinic-orbit bifurcation (HC). (b) Three-dimensional representation in the space $[S, \rho\cos(\phi), \rho\sin(\phi)]$ disclosing the bursting regime. Parameters are $\omega_0 = 1.8$, $\Delta = 1.4$, $\alpha = 5.0$, $\varepsilon = 0.01$, $K = 7.41$.

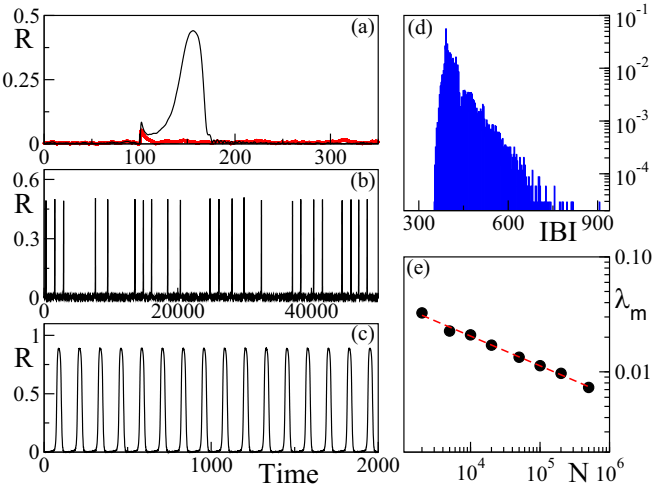

FIG. 4. Time series of $R(t)$ for the unimodal KMI: (a) $K = 4.5$ (excitable response); (b) $K = 4.75$ (irregular bursting); (c) $K = 10.3$ (periodic bursting). For $K = 4.75$ we report also the interburst interval (IBI) distribution for $N = 20\,000$ (d) and the maximal Lyapunov exponent vs N (e). The red dashed line in (e) refers to a power-law fitting with exponent $\simeq 0.259$. Other parameters: $N = 500\,000$, $m = 2$, $\varepsilon = 0.01$, $\alpha = 30$.

with a solution of Eqs. (2a)–(2c) in the bursting regime (blue solid line).

Starting, e.g., from a PS initial condition, the motion is rapidly attracted by Σ_S. Since Eq. (2c) dictates that S is always decreasing on the curve $\mathcal{F}(\rho_s)$ [see Fig. 3(a)], the system is driven towards the fold point F, where it forcibly leaves the critical manifold turning on the fast dynamics transversal to it. When the trajectory enters the region in which the fast subsystem has a stable limit cycle [green lines in Fig. 3(a) and shaded area in Fig. 3(b)], the slow monotonic evolution translates into a sequence of nearly periodic spikes. Such an oscillatory state persists until it collides with the repelling part of the manifold where it disappears via a saddle homoclinic-orbit bifurcation (HC). Since Σ_R repels all neighboring trajectories, while Σ_S attract them, the motion is driven back to the upper state where a new bursting cycle begins. Interestingly, the transition from the spiking activity to the upper state exhibits the typical features of canard explosions [38,39]: Due to the finiteness of ε, the trajectories close to Σ_R do not jump immediately to Σ_S, but continue moving on the slow timescale along the unstable portion of the manifold for a certain amount of time [see the inset in Fig. 3(a)]. A more detailed analysis can be found in the Supplemental Material [31].

The above scenario is known as *fold-homoclinic* bursting [12]: It has been found in several low-dimensional neuron models, including, e.g., the Hindmarsh-Rose [13], the Morris-Lecar with current-feedback control [12], a modified FitzHugh-Nagumo [40], the Chay model [41,42], a one-compartment model of a Purkinje cell dendrite [43], and a pancreatic β-cell model [16].

Excitability and chaotic bursting can be explained on the same basis: When the system is in the regime of quasi-harmonic oscillations, either periodic or chaotic, an external perturbation or a sufficiently large chaotic fluctuation can trigger the fast dynamics, giving rise to an excursion to the upper stable branch Σ_S before returning to the initial state [44–46].

Dynamics of the KMI network. To further support the generality of the phenomenon, we now consider a KMI with mass $m = 2$ and natural frequencies distributed according to either a unimodal or a bimodal Gaussian distribution.

Typical time traces of $R(t)$ for the KMI with a unimodal distribution centered in zero and with a unitary standard deviation are plotted in Fig. 4 for different values of K. In this case we observe collective excitability and *fold-fold* bursting [12], but there is no trace of spiking dynamics. This is probably due to the fact that the fast subsystem displays a hysteretic transition from an AS to a PS regime, but no evidence of standing waves as in the previous case. We have found irregular busting at low K ($4.6 \lesssim K \lesssim 7$), as shown in Fig. 4(b), and periodic bursting for sufficiently large $K \gtrsim 7$ [see Fig. 4(c)]. The erraticity in the bursting dynamics is confirmed by the distribution of the interburst intervals (IBIs) among successive bursts, which displays a clear exponential tail characteristic of Poissonian processes shown in Fig. 4(d). The origin of the irregular bursting is related to a weak form of chaos induced by finite-size fluctuations [47]. Indeed, the maximal Lyapunov exponent vanishes in the thermodynamic limit as $\lambda_m \propto N^{-1/4}$, as shown in Fig. 4(e).

As a final example, we consider a KMI population with a bimodal distribution composed of two almost nonoverlapping Gaussians centered at $\omega_0 = \pm 2$ and with unitary standard deviations [26]. In this case we still observe regimes of irregular bursting due to finite-size effects ($8.5 \lesssim K \lesssim 10$). Indeed, as shown in Figs. 5(a)–5(c), the bursts become rarer for increasing N, while the maximal Lyapunov exponent vanishes as $\lambda_m \propto N^{-1/3}$ [see Fig. 5(d)]. Besides this regime, for larger K, we can also have periodic bursting. However, the oscillations now emerge on the top of the burst, as shown in Fig. 5(e), due to the coexistence of standing waves with the PS regime for the fast subsystem as found in Ref. [26]. These bursts

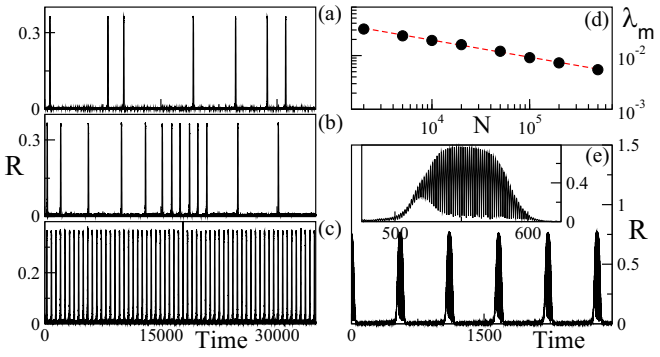

FIG. 5. Time series of $R(t)$ for the bimodal KMI. Erratic busting behavior is reported in (a)–(c) at $K = 9.45$ for increasing system sizes: (a) $N = 100\,000$, (b) 200 000, and (c) 500 000. The corresponding maximal Lyapunov exponent λ_m is reported in (d) vs N, and the dashed red line refers to a power-law fitting with exponent $\simeq$0.318. In (e), $R(t)$ is displayed vs time for $K = 10.3$ and $N = 200\,000$; an enlargement is shown in the inset. Other parameters: $m = 2$, $\varepsilon = 0.01$, $\alpha = 30$.

resemble the so-called *Hopf-Hopf* bursting reported in Ref. [12]. Similar bursting is also observed in the unimodal KMI for large masses.

Conclusions. Our analysis indicates the minimal ingredients for the emergence of collective excitability and bursting oscillations in populations of rotators with adaptive coupling. The network dynamics without feedback, corresponding to the fast subsystem, must display a hysteretic phase transition connecting a low synchronization state to one with a higher synchronization degree. The global feedback equation (slow subsystem) introduces a state-dependent modulation of a control parameter (in our case, the coupling strength), driving the system across the hysteresis cycle.

For the bimodal KM, an exact mean-field formulation can be derived consisting of a three-dimensional (3D) system with two fast and one slow variable. A detailed geometric singular perturbation analysis of this model allows us to explain collective excitability in terms of the stability properties of a 1D slow invariant manifold [31]. This demonstrates that the phenomenon persists in the thermodynamic limit and it is not related to finite-size effects [9] for this autonomous model we have shown the existence of different types of collective chaos (namely, chaotic spiking and bursting) and characterized in detail the transition between the two chaotic regimes. The reported dynamical macroscopic scenario is fairly reminiscent of that observed for the Hindmarsh-Rose model for a single neuron [15,17,18]. This analogy paves the way for the application of our results in the context of computational neurosciences.

For what concerns the KMI, we observe only bursting dominated phases, which can be weakly chaotic, but in the thermodynamic limit we expect regular trains of fold-fold or Hopf-Hopf bursts [12] only. As shown in a previous analysis [26], for sufficiently large masses, the KMI (in the absence of feedback) can become chaotic, therefore for $m \gg 1$, we expect chaotic bursting regimes to appear also for this model.

The exact reduction techniques developed for networks of phase oscillators [7,30] do not apply to the KMI. In the latter case, a promising approach to investigate, in order to derive a low-dimensional mean-field description, is the so-called circular cumulant expansion, recently applied with success to noisy oscillator populations [48] and to stochastic systems with small inertia [49].

Acknowledgments. We acknowledge Veronica and Milena Marino for lively and animated discussions. A.T. received financial support by the Excellence Initiative I-Site Paris Seine (Grant No. ANR-16-IDEX-008), by the Labex MME-DII (Grant No. ANR-11-LBX-0023-01), and by the ANR Project ERMUNDY (Grant No. ANR-18-CE37-0014), all part of the French program Investissements d'Avenir.

[1] Y. Kuramoto, *Chemical Oscillations, Waves, and Turbulence* (Courier Corporation, North Chelmsford, MA, 2003).
[2] A. Pikovsky, M. Rosenblum, and J. Kurths, *Synchronization: A Universal Concept in Nonlinear Sciences*, Vol. 12 (Cambridge University Press, Cambridge, UK, 2003).
[3] J. A. Acebrón, L. L. Bonilla, C. J. P. Vicente, F. Ritort, and R. Spigler, Rev. Mod. Phys. **77**, 137 (2005).
[4] P. C. Matthews and S. H. Strogatz, Phys. Rev. Lett. **65**, 1701 (1990).
[5] V. Hakim and W.-J. Rappel, Phys. Rev. A **46**, R7347 (1992).
[6] N. Nakagawa and Y. Kuramoto, Prog. Theor. Phys. **89**, 313 (1993).
[7] E. Ott and T. M. Antonsen, Chaos **18**, 037113 (2008).
[8] P. So and E. Barreto, Chaos **21**, 033127 (2011).
[9] P. S. Skardal, D. Taylor, and J. G. Restrepo, Physica D **267**, 27 (2014).
[10] H. C. Tuckwell, *Introduction to Theoretical Neurobiology, Vol. 1: Linear Cable Theory and Dendritic Structure* (Cambridge University Press, Cambridge, UK, 1988).
[11] C. Kock, *Biophysics of Computation* (Oxford University Press, Oxford, UK, 1999).
[12] E. M. Izhikevich, Int. J. Bifurcation Chaos **10**, 1171 (2000).
[13] J. L. Hindmarsh and R. Rose, Proc. R. Soc. London, Ser. B. Biol. Sci. **221**, 87 (1984).
[14] D. Terman, J. Nonlinear Sci. **2**, 135 (1992).
[15] X.-J. Wang, Physica D **62**, 263 (1993).
[16] E. Mosekilde, B. Lading, S. Yanchuk, and Y. Maistrenko, BioSystems **63**, 3 (2001).
[17] J. M. González-Miranda, Chaos **13**, 845 (2003).
[18] G. Innocenti, A. Morelli, R. Genesio, and A. Torcini, Chaos **17**, 043128 (2007).
[19] S. Coombes and P. Bressloff, *Bursting: The Genesis of Rhythm in the Nervous System* (World Scientific, Singapore, 2005).
[20] E. Meron, Phys. Rep. **218**, 1 (1992).
[21] M. Ciszak, A. Montina, and F. T. Arecchi, Chaos **19**, 015104 (2009).
[22] A. Dolcemascolo, A. Miazek, R. Veltz, F. Marino, and S. Barland, Phys. Rev. E **101**, 052208 (2020).

[23] Standing waves emerge when two synchronized clusters of rotators oscillate with opposite angular velocity.
[24] D. Pazó and E. Montbrió, Phys. Rev. E **80**, 046215 (2009).
[25] H.-A. Tanaka, A. J. Lichtenberg, and S. Oishi, Phys. Rev. Lett. **78**, 2104 (1997).
[26] S. Olmi and A. Torcini, *Control of Self-Organizing Nonlinear Systems* (Springer, Berlin, 2016), pp. 25–45.
[27] Y. Kuramoto, *International Symposium on Mathematical Problems in Theoretical Physics* (Springer, Berlin, 1975), pp. 420–422.
[28] S. Olmi, A. Navas, S. Boccaletti, and A. Torcini, Phys. Rev. E **90**, 042905 (2014).
[29] The frequencies have been generated deterministically following the procedure reported in Ref. [50], which allows one to uniformly cover the range of possible frequencies. However, our results are not modified by considering other frequency distributions, e.g., bimodal Lorentzian or Gaussian.
[30] E. A. Martens, E. Barreto, S. H. Strogatz, E. Ott, P. So, and T. M. Antonsen, Phys. Rev. E **79**, 026204 (2009).
[31] See Supplemental Material at http://link.aps.org/supplemental/10.1103/PhysRevE.102.050201 for the derivation of the mean-field equations (2) and its singular perturbation analysis, for the maximal Lyapunov exponent estimation of the mean-field model, as well as for details on the numerical simulations.
[32] A. Pikovsky and A. Politi, *Lyapunov Exponents: A Tool to Explore Complex Dynamics* (Cambridge University Press, Cambridge, U.K., 2016).
[33] T. Shibata and K. Kaneko, Phys. Rev. Lett. **81**, 4116 (1998).
[34] S. Olmi, A. Politi, and A. Torcini, Europhys. Lett. **92**, 60007 (2011).
[35] C. Bick, M. J. Panaggio, and E. A. Martens, Chaos **28**, 071102 (2018).
[36] M. W. Hirsch, R. L. Devaney, and S. Smale, *Differential Equations, Dynamical Systems, and Linear Algebra*, Vol. 60 (Academic, New York, 1974).
[37] N. Fenichel, J. Diff. Equ. **31**, 53 (1979).
[38] J.-L. Callot, F. Diener, and M. Diener, C. R. Acad. Sci. Paris, Ser. I **286**, 1059 (1978).
[39] E. Benoit, J.-F. Callot, F. Diner, and M. Diener, Collect. Math. **32**, 37 (1981).
[40] J. Alidousti and R. K. Ghaziani, Math. Models Comput. Simul. **9**, 390 (2017).
[41] T. R. Chay, Physica D **16**, 233 (1985).
[42] Z. Yang, Q. Lu, and L. Li, Chaos, Solitons Fractals **27**, 87 (1981).
[43] Y. Mandelblat, Y. Etzion, Y. Grossman, and D. Golomb, J. Comput. Neurosci. **11**, 43 (2001).
[44] F. Marino, F. Marin, S. Balle, and O. Piro, Phys. Rev. Lett. **98**, 074104 (2007).
[45] K. Al-Naimee, F. Marino, M. Ciszak, R. Meucci, and F. T. Arecchi, New J. Phys. **11**, 073022 (2009).
[46] K. Al-Naimee, F. Marino, M. Ciszak, S. Abdalah, R. Meucci, and F. Arecchi, Eur. Phys. J. D **58**, 187 (2010).
[47] O. V. Popovych, Y. L. Maistrenko, and P. A. Tass, Phys. Rev. E **71**, 065201(R) (2005).
[48] I. V. Tyulkina, D. S. Goldobin, L. S. Klimenko, and A. Pikovsky, Phys. Rev. Lett. **120**, 264101 (2018).
[49] D. S. Goldobin and L. S. Klimenko, in *28th Russian Conference on Mathematical Modelling in Natural Sciences*, edited by V. P. Matveenko, P. V. Trusov, A. Yu. Yants, and V. A. Faerman, AIP Conf. Proc. No. 2216 (AIP, Melville, NY, 2020), p. 070001.
[50] E. Montbrió, D. Pazó, and A. Roxin, Phys. Rev. X **5**, 021028 (2015).